Cellular/Molecular

Protein Kinase G Dynamically Modulates TASK1-Mediated Leak K^+ Currents in Cholinergic Neurons of the Basal Forebrain

Hiroki Toyoda,[1]* Mitsuru Saito,[1]* Makoto Okazawa,[2]* Keiko Hirao,[1] Hajime Sato,[1] Haruka Abe,[2] Kenji Takada,[1] Kazuo Funabiki,[2] Masahiko Takada,[3] Takeshi Kaneko,[4] and Youngnam Kang[1]

[1]Department of Neuroscience and Oral Physiology, Osaka University Graduate School of Dentistry, Suita, Osaka 565-0871, Japan, [2]Department of Systems Biology, Osaka Bioscience Institute, Suita, Osaka 565-0874, Japan, [3]Systems Neuroscience Section, Primate Research Institute, Kyoto University, Inuyama, Aichi 484-8506, Japan, and [4]Department of Morphological Brain Science, Graduate School of Medicine, Kyoto University, Kyoto 606-8501, Japan

Leak K^+ conductance generated by TASK1/3 channels is crucial for neuronal excitability. However, endogenous modulators activating TASK channels in neurons remained unknown. We previously reported that in the presumed cholinergic neurons of the basal forebrain (BF), activation of NO-cGMP-PKG (protein kinase G) pathway enhanced the TASK1-like leak K^+ current (I-K_{leak}). As 8-Br-cGMP enhanced the I-K_{leak} mainly at pH 7.3 as if changing the I-K_{leak} from TASK1-like to TASK3-like current, such an enhancement of the I-K_{leak} would result either from an enhancement of hidden TASK3 component or from an acidic shift in the pH sensitivity profile of TASK1 component. In view of the report that protonation of TASK channel decreases its open probability, the present study was designed to examine whether the activation of PKG increases the conductance of TASK1 channels by reducing their binding affinity for H^+, i.e., by increasing K_d for protonation, or not. We here demonstrate that PKG activation and inhibition respectively upregulate and downregulate TASK1 channels heterologously expressed in PKG-loaded HEK293 cells at physiological pH, by causing shifts in the K_d in the acidic and basic directions, respectively. Such PKG modulations of TASK1 channels were largely abolished by mutating pH sensor H98. In the BF neurons that were identified to express ChAT and TASK1 channels, similar dynamic modulations of TASK1-like pH sensitivity of I-K_{leak} were caused by PKG. It is strongly suggested that PKG activation and inhibition dynamically modulate TASK1 currents at physiological pH by bidirectionally changing K_d values for protonation of the extracellular pH sensors of TASK1 channels in cholinergic BF neurons.

Introduction

Leak K^+ (K_{leak}) channels are known to be the major determinants of the resting membrane potential and input resistance. TWIK-related acid-sensitive K^+ (TASK) channels, TASK1/3, are the most likely candidates for K_{leak} channels in various central neurons (Millar et al., 2000; Sirois et al., 2000; Talley et al., 2000; Meuth et al., 2003). TASK1 channels are inhibited by various neurotransmitters through the activation of G-protein-coupled receptors (Bayliss et al., 2003; Lesage, 2003). By contrast, endogenous neuromodulators opening TASK1 channels remain unknown, although the volatile anesthetics are known to open TASK1 channels (Bayliss et al., 2003; Lesage, 2003).

Recently, we have reported that the activation of NO-cGMP-PKG (protein kinase G) pathway upregulates the K_{leak} current (I-K_{leak}), which is similar to TASK1 currents in its extracellular pH sensitivity, in the presumed cholinergic neurons of the basal forebrain (BF) (Kang et al., 2007; Toyoda et al., 2008). The enhancement of the I-K_{leak} by PKG activation was seen at pH 7.3 but not at pH 6.3 and 8.3, as if PKG changes the pH sensitivity of the I-K_{leak} from the one similar to that of TASK1 to the other similar to that of TASK3 current (Toyoda et al., 2008). Such an enhancement of the I-K_{leak} would result either from an enhancement of hidden TASK3 component or from an acidic shift in the pH sensitivity profile of TASK1 component of the I-K_{leak}. Since the protonation of the possible or identified pH sensors of TASK1 channels decreases TASK1 currents (Kim et al., 1999; Lopes et al., 2001; Morton et al., 2003), we hypothesized that the activation of PKG increased the I-K_{leak} by reducing the binding affinity of the TASK1 channels for H^+, thereby shifting the pH sensitivity profile of the I-K_{leak} in the acidic direction.

To directly address this hypothesis, in the present study, we first investigated whether and how PKG modulates cloned TASK1 channels and its mutations of the pH sensors, H98N and K210N, heterologously expressed in HEK cells. Second, we examined whether the pH sensitivity of the I-K_{leak} in the identified cholinergic BF neurons is dynamically modulated depending on the level of PKG activity or not. We found that PKG activation and inhibition respectively upregulate and downregulate TASK1 channels expressed in PKG-loaded HEK cells at physiological pH, by bidirectionally shifting the pH sensitivity profile. Such PKG modulations of TASK1 channels were largely abolished in H98N

Received Nov. 1, 2009; revised Feb. 6, 2010; accepted March 14, 2010.

This work was supported by Grant-in-Aid for Scientific Research on Priority Areas (A) No. 20021019 from the Ministry of Education, Culture, Sports, Science and Technology of Japan to Y.K. and also partly supported by a donation from Lotte Co., Ltd. (Tokyo, Japan) to Y.K.

*H.T., M.S., and M.O. contributed equally to this work.

Correspondence should be addressed to Dr. Youngnam Kang, Department of Neuroscience and Oral Physiology, Osaka University Graduate School of Dentistry, 1-8, Yamadaoka, Suita, Osaka 565-0871, Japan. E-mail: kang@dent.osaka-u.ac.jp.

DOI:10.1523/JNEUROSCI.5407-09.2010

 0270-6474/10/305677-13$15.00/0

and decreased in K210N mutations. Similar to those seen in wild-type (WT) TASK1 channels, bidirectional shifts in the TASK1-like pH sensitivity of the I-K_{leak} were caused by PKG activation and inhibition in cholinergic BF neurons that express TASK1 channels. These results suggest that the PKG activation and inhibition changed the K_d values for protonation of the extracellular pH sensors of TASK1 channels, leading to a dynamic modulation of TASK1 currents at physiological pH in cholinergic BF neurons.

Materials and Methods

Heterologous expression of TASK1 in HEK293 cells. The entire coding region and flanking regions of TASK1 were amplified by PCR from mouse fetal Marathon-Ready cDNA (Clontech/Takara Bio) with 5′-GTGGTGCTGAAGGGACAGATCC-3′ and 5′-AAGGGAGTGGACACGTAAGG-3′ and subcloned into pCR-Blunt II-TOPO vector (Invitrogen) to generate pCR-TASK1. The complete coding sequence of TASK1 was amplified by PCR using pCR-TASK1 as a template with 5′-ACTCAGATCTCGAGCCGCCACCATGAAGCGGCAGAATGTG-3′ and 5′-CGGATCCCGGGCCCTCACACCGAGCTCCTGCGCTTC-3′. The PCR fragment was digested with BglII and ApaI, and subcloned into BamHI and ApaI sites of pcDNA5/FRT/TO vector (Invitrogen), to generate pcDNA5/FRT/TO-TASK1. Mutagenesis was performed using the QuikChange Site-Directed Mutagenesis Kit (Stratagene) according to the manufacturer's instructions. pcDNA5/FRT/TO-TASK1 was used as a template. The mutagenic primers used were as follows: TASK1 H98N, sense 5′-CCATCGGCTATGGTAATGCGGCGCCCAG-3′, antisense 5′-CTGGGCGCCGCATTACCATAGCCGATGG-3′; TASK1 K210N, sense 5′-CTATGTGGCGCTGCAGAATGACCAGGCGC-3′; antisense 5′-GCGCCTGGTCATTCTGCAGCGCCACATAG-3′. WT and mutated TASK1 were subcloned into XhoI and SmaI sites of pIRES2-ZsGreen1 vector (Clontech/Takara Bio), to generate pIRES2-ZsGreen1-TASK1, pIRES2-ZsGreen1-TASK1 H98N, and pIRES2-ZsGreen1-TASK1 K210N. Inserted sequences of all plasmid constructs were verified by DNA sequencing.

For stable inducible expression of TASK1, parental Flp-In T-REx-293 cells (Invitrogen) were cultured in DMEM supplemented with 10% FBS, 100 U/ml penicillin, 100 μg/ml streptomycin, 15 μg/ml blasticidin, and 100 μg/ml zeocin at 37°C in 5% CO_2. pcDNA5/FRT/TO-TASK1 or the empty vector pcDNA5/FRT/TO (mock) was cotransfected into Flp-In T-REx-293 cells with pOG44 plasmid (Invitrogen) encoding flp recombinase by using Lipofectamine 2000 (Invitrogen). Stably transfected, hygromycin-resistant cells were selected using 150 μg/ml hygromycin B instead of zeocin. For induction of TASK1 expression, the stably transfected Flp-In T-REx 293 cells plated on glass coverslips were treated with 1 μg/ml doxycycline (Clontech/Takara Bio) for 12–48 h before electrophysiological recording. For transient expression of TASK1 and TASK1 mutants, 293A cells (Invitrogen) cultured in DMEM supplemented with 10% FBS, 100 U/ml penicillin, 100 μg/ml streptomycin were transfected with pIRES2-ZsGreen1-TASK1 (or TASK1 mutants) by using Lipofectamine LTX (Invitrogen). One day after transfection, cells were plated onto glass coverslips. Electrophysiological recording was performed 36–60 h after transfection.

Slice preparation. The procedure for slice preparation was the same as that in our previous studies (Kang et al., 2007; Toyoda et al., 2008). Using 12–16 d postnatal Wistar rats of both sexes (Charles River Breeders), slices of 300 μm thickness were cut coronally from the most rostral portion of BF containing the nuclei of medial septum/diagonal band (MS/DB). All experiments were performed in accordance with the guidelines of Osaka University Graduate School of Dentistry for the care and use of laboratory animals.

Electrophysiological recording. The electrophysiological studies were performed on HEK cells and neurons identified as type II based on the characteristic late-spiking pattern due to A-like K^+ current in the MS/DB nuclei (Griffith and Matthews, 1986; Markram and Segal, 1990; Kang et al., 2007). Axopatch 200B (MDS Analytical Technologies) was used for the whole-cell patch-clamp recording. The standard extracellular solution had the following composition (in mM): 124 NaCl, 1.8 KCl, 2.5 $CaCl_2$, 1.3 $MgCl_2$, 26 $NaHCO_3$, 1.2 KH_2PO_4, 10 glucose, bubbled with a mixture of 95% O_2–5% CO_2. When changing the extracellular pH from 7.3 to more acidic or basic values, 26 mM $NaHCO_3$ was substituted with 10 mM HEPES and 12 mM NaCl in the extracellular solution bubbled with 100% O_2, and the pH was adjusted using NaOH (Talley et al., 2000). This is because the manipulation of pH is easy in the HEPES-buffered solution, while the brain slice could be maintained better in the physiological bicarbonate buffer. There was no significant difference in the leak K^+ current between cholinergic BF neurons bathed in the bicarbonate- and HEPES-buffered extracellular solutions, consistent with the report on TASK-like K^+ channels in rat dorsal vagal neurons (Hopwood and Trapp, 2005). All the recordings of HEK cells were obtained in the HEPES-buffered solution. The internal solution had the following composition (in mM): 123 K-gluconate, 8 KCl, 20 NaCl, 0.5 $MgCl_2$, 0.5 ATP-Na_2, 0.3 GTP-Na_3, 10 HEPES, 0.1 EGTA; the pH was adjusted to 7.3 with KOH. The patch pipettes had a DC resistance of 4–5 MΩ when filled with the internal solution. The membrane potential values given in the text were corrected for the junction potential between the internal solution (negative) and the standard extracellular solution (10 mV). All recordings were made at room temperature (20–24°C). The sealing resistance was usually >10 GΩ. Whole-cell currents or voltages were low pass filtered at 2 kHz (four-pole Bessel filter), digitized at a sampling rate of 2–10 kHz (Digidata 1322A, MDS Analytical Technologies). Under the voltage-clamp condition at the holding potential of −70 mV, step (to −90 mV, 0.1 s duration) and depolarizing ramp (−130 to −50 mV, 0.9 s duration) pulses (step-and-ramp pulses) were applied alternately every 10 s. The conductance was measured using linear regression across the linear part of the current–voltage (I–V) plot (−70 to −95 mV) in response to the ramp pulse.

Numerical data were expressed as the mean ± SD. The statistical significance was assessed using paired (†) or unpaired (‡) Student's t test and ANOVA (§) followed by Fisher's protected least significant difference *post hoc* test. $p < 0.05$ was considered statistically significant.

Drug application. 8-Bromoguanosine-3′,5′-cyclomonophosphate (8-Br-cGMP, a membrane-permeable cGMP analog, Sigma-Aldrich) and Rp-8-bromo-β-phenyl-1,N^2-ethenoguanosine 3′,5′-cyclic monophosphorothioate sodium salt [Rp-8-Br-PET-cGMPS (Rp-PET), a membrane-permeable PKG inhibitor, Sigma-Aldrich] were bath applied at concentrations of 100–200 μM and 10–20 μM, respectively. KT5823 (a membrane-permeable PKG inhibitor, Calbiochem) was dissolved in DMSO for preparing stock solution and was bath applied at a dilution of 1/1000 to give a final concentration of 2 μM. KT5823 interferes with ATP for binding to the catalytic domain of PKG (Hidaka and Kobayashi, 1992), while Rp-8-Br-PET-cGMPS competes with cGMP for a common binding site of the regulatory domain of PKG (Butt et al., 1995). Recombinant PKGIα (Promega) or PKGII (Sigma-Aldrich) at a concentration of 400 units/ml (1 unit will hydrolyze 1 pmol of substrate) was added to the pipette solution. As a negative control, PKGII inactivated by boiling at 95°C for at least 15 min was applied to the pipette solution.

Single-cell RT-PCR. After whole-cell recording in a type II neuron, its intracellular content was aspirated into a patch pipette under visual control and was gently put into a reaction tube containing RT agents. RT was performed for 1 h at 37°C (Sensicript RT, Qiagen). Subsequently, PCR amplification was performed in the reaction mixture (30 μl) composed of 10× PCR buffer, 2.5 mM $MgCl_2$, 0.2 mM each deoxyribonucleotide triphosphate, 1.0 μM each primer, 2 unit HotStarTaq DNA polymerase (Qiagen), and 2 μl RT reaction product, through the following series of reactions: 94°C, 15 min, 35 cycles (93°C, 1 min; 55°C, 1 min; 72°C, 1 min), and 72°C, 5 min in a thermal cycler (GeneAmp PCR System 9700, Applied Biosystems). In some cases, 1 μl of the first-round PCR product was used for the second-round PCR with 30 cycles. For PCR amplifications, the following primers were used: TASK1 (nucleotides 220-735, accession number AB048823), sense CACCGTCATCACCACAATCG, antisense TGCTCTGCATCACGCTTCTC (Meuth et al., 2003); TASK3 (nucleotides 188-602, accession number AF192366), sense ATGAGATGCGCGAGGAGGAGAAAC, antisense ACGAGGCCCATGCAAGAAAAGAAG (Meuth et al., 2003); ChAT (nucleotides 1729-2052), sense ATGGCCATTGACAACCATCTTCTG, antisense CCTTGAACTGCAGAGGTCTCTCAT (Brice et al., 1989). All the primers were obtained from Sigma Genosys. Aliquots of the PCR products were analyzed by 2%

agarose gel electrophoresis (Nacalai Tesque) and visualized using ethidium bromide. The PCR product was run in parallel with known molecular weight markers (100 bp ladder, Bio-Rad). As a positive control, single-cell RT-PCR was performed on neurons in the trigeminal motor nucleus (TMN) of rats at postnatal days 7–10 because TASK1 and TASK3 mRNAs are known to be highly expressed in TMN (Talley et al., 2001). The amplified PCR fragments were in accordance with the respective lengths predicted by the two subunit primers in all of 13 TMN neurons examined (see Fig. 5*C*).

Fluorescence immunohistochemistry. For immunostaining of stable transfected cell lines, doxycycline-treated cells on coverslips were fixed for 10 min with ice-cold methanol/acetone (1:1) at −20°C. After blocking with 2% normal goat serum (Vector Laboratories) in PBS for 1 h, cells were incubated with 1 μg/ml of affinity-purified anti-[human TASK1 (K_{2P}3.1) residues 252–269] rabbit antibody (Alomone Laboratories) overnight at 4°C. Cells were washed with PBS, followed by 1 h incubation at room temperature with Alexa Fluor 488-conjugated anti-[rabbit IgG] goat antibody (Invitrogen).

For immunostaining of cholinergic BF neurons and TMN neurons, fixed brains were prepared from three Wistar rats following the protocol described in the previous studies (Furuta et al., 2004; Saito et al., 2006). The 40-μm-thick coronal sections containing the MS/DB nuclei and the TMN were incubated overnight in PBS containing 0.3% (v/v) Triton X-100, 0.25% (w/v) λ-carrageenan and 1% (v/v) donkey serum with a mixture of 1:500-diluted anti-ChAT goat antiserum (AB144P, Millipore Bioscience Research Reagents) or 1:500-diluted anti-NeuN mouse monoclonal antibody (MAB377, Millipore Bioscience Research Reagents) and 1 μg/ml of affinity-purified anti-[human TASK1 (K_{2P}3.1) residues 252–269] or anti-[rat TASK3 (K_{2P}9.1) residues 57–73] rabbit antibody (Alomone Laboratories). After a wash with PBS containing 0.3% Triton X-100, the sections were incubated for 1 h with 10 μg/ml biotinylated anti-[rabbit IgG] donkey antibody (Millipore Bioscience Research Reagents), and then for 1 h with 10 μg/ml Alexa Fluor 488-conjugated anti-[goat IgG] donkey antibody (Invitrogen) and Cy3-conjugated streptavidin (Invitrogen) in the presence of 10% (v/v) normal rabbit serum. For control experiments, when one of the primary antibodies was omitted or replaced with normal IgG or serum, no immunofluorescence for the omitted or replaced antibody was detected. For the absorption tests for anti-TASK1 and anti-TASK3 antibodies, the primary antibody solution was preincubated for 1 h with the antigen peptide (1 μg peptide for 1 μg antibody) before the incubation with sections (see supplemental information and supplemental Fig. 1*A*, available at www.jneurosci.org as supplemental material, for TASK1 absorption test). The sections were observed with a confocal laser-scanning microscope (LSM510, Zeiss). Alexa Fluor 488 and Cy3 were excited with 488 and 543 nm laser beams and observed through 505–530 nm and >560 nm emission filters, respectively. The digital images were captured by using a software (LSM510, Zeiss).

Results

Basal TASK1 currents in HEK293 cells enhanced by PKG loading

Immunoreactivities for TASK1 were examined to verify the expression of TASK1 channels in HEK293 cells induced by doxycycline treatment (see Materials and Methods). The presence of HEK cells in each experiment can be seen in the bright-field photomicrographs shown on the bottom (Fig. 1*A*). In the HEK cells transfected with TASK1, unambiguous immunoreactivity was clearly seen along the plasma membrane and partly in the cytoplasm (Fig. 1*Aa*, top). In contrast, the HEK cells transfected with mock displayed no intense immunoreactivity more than diffuse background fluorescence (Fig. 1*Ab*, top). Furthermore, when the primary antibody against TASK1 was omitted, HEK cells transfected with TASK1 also displayed no intense immunoreactivity (Fig. 1*Ac*, top).

Since the expression level of PKG protein in WT HEK cells is low (Kwan et al., 2004), recombinant PKGII or PKGIα was included in the pipette solution (White et al., 2000) to examine the effects of PKG activator and inhibitor on TASK1 currents. First, effects of PKG loading itself on the basal TASK1 current were examined.

In response to ramp pulses, both the PKG-unloaded and PKGII-loaded mock-transfected cells displayed small inwardly rectifying currents (Fig. 1*Ba*, upper and lower traces, respectively), which are distinct from outwardly rectifying TASK1 current. There was no apparent pH-sensitive K^+ current as revealed by the superimposed traces of the current responses obtained at various pHs in the PKG-unloaded and PKGII-loaded mock-transfected HEK cells (Fig. 1*Ba*, upper and lower traces, respectively). In the PKG-unloaded mock-transfected HEK cells ($n = 5$), there were no significant (§) differences in the mean conductance normalized to those at pH 6.3 among the current responses obtained at pH 6.3, at pH 7.3, and at pH 8.3 (Fig. 1*Bb*, open columns). Similarly, in the PKGII-loaded mock-transfected HEK cells ($n = 8$), there were no significant (§) differences in the mean conductance normalized to those at pH 6.3 among the current responses obtained at pH 6.3, at pH 7.3 and at pH 8.3 (Fig. 1*Bb*, gray columns). These results suggest that PKGII loading itself had almost no effect on the intrinsic channel activity of HEK cells, which was insensitive to external pH.

Both in the PKG-unloaded and PKGII-loaded HEK cells transfected with TASK1 (Fig. 1*Ca*,*Cb*, respectively), respective current responses to the ramp pulse obtained at pH 8.3, 7.3, and 6.3 crossed each other around the theoretical K^+ equilibrium potential ($E_K = -95$ mV), and displayed the Goldman–Hodgkin–Katz (GHK)-type outward rectification (Fig. 1*Ca*,*Cb*, dotted curves). The mean value of conductances at pH 7.3 normalized to that at pH 6.3 (N-$G_{7.3}$) in the PKGII-loaded HEK cells (2.1 ± 0.3, $n = 6$) was slightly but significantly (‡) larger than that obtained in the PKG-unloaded ones (1.8 ± 0.2, $n = 5$), while the mean value of N-$G_{8.3}$ in the PKGII-loaded ones (4.1 ± 0.4, $n = 6$) was not significantly (‡) different from that in the PKG-unloaded ones (3.7 ± 0.6, $n = 5$) (Fig. 1*Da*).

The pH sensitivity of TASK1 currents between pH 6.3 and 8.3 can be well represented as the scaled conductance (S-G_x) as defined in our previous study (Toyoda et al., 2008): $\text{S-}G_x = (G_x - G_{6.3})/(G_{8.3} - G_{6.3})$, where x is the pH of the external solution. The pH profile of the scaled conductances (Fig. 1*Db*) is consistent with the pH sensitivity of TASK1 currents reported previously (Kang et al., 2004). The mean value of S-$G_{7.3}$ in the PKGII-loaded HEK cells (0.35 ± 0.05, $n = 6$) was slightly but significantly (‡) larger than that obtained in the PKG-unloaded ones (0.28 ± 0.06, $n = 5$) (Fig. 1*Db*, gray and open columns). These results indicate that TASK1 currents heterologously expressed in HEK cells at pH 7.3 were only slightly enhanced by loading of PKGII, which were presumably activated by endogenous cGMP that might be limitedly produced by the limited activity of soluble guanylyl cyclase (sGC) from GTP supplied from the patch pipette.

Modulation of TASK1 currents in PKG-loaded HEK cells by 8-Br-cGMP

In the PKG-unloaded HEK cells, 100 μM 8-Br-cGMP only slightly increased the TASK1 current (Fig. 2*Aa*,*Ab*, compare **1* and **2*; see also Fig. 2*C*), whereas the subsequent pH increase to 8.3 in the absence of 8-Br-cGMP markedly increased the TASK1 current (Fig. 2*Aa*,*Ab*, compare **2* and **3*). This could be more clearly seen in the changes in the conductance, which is reflected in peak level (Fig. 2*Aa*, arrowheads) of respective current responses when referred to the zero current level. These observations suggest that 8-Br-cGMP was not so effective due to the paucity of intrinsic PKG in HEK cells. Indeed in the PKGII-

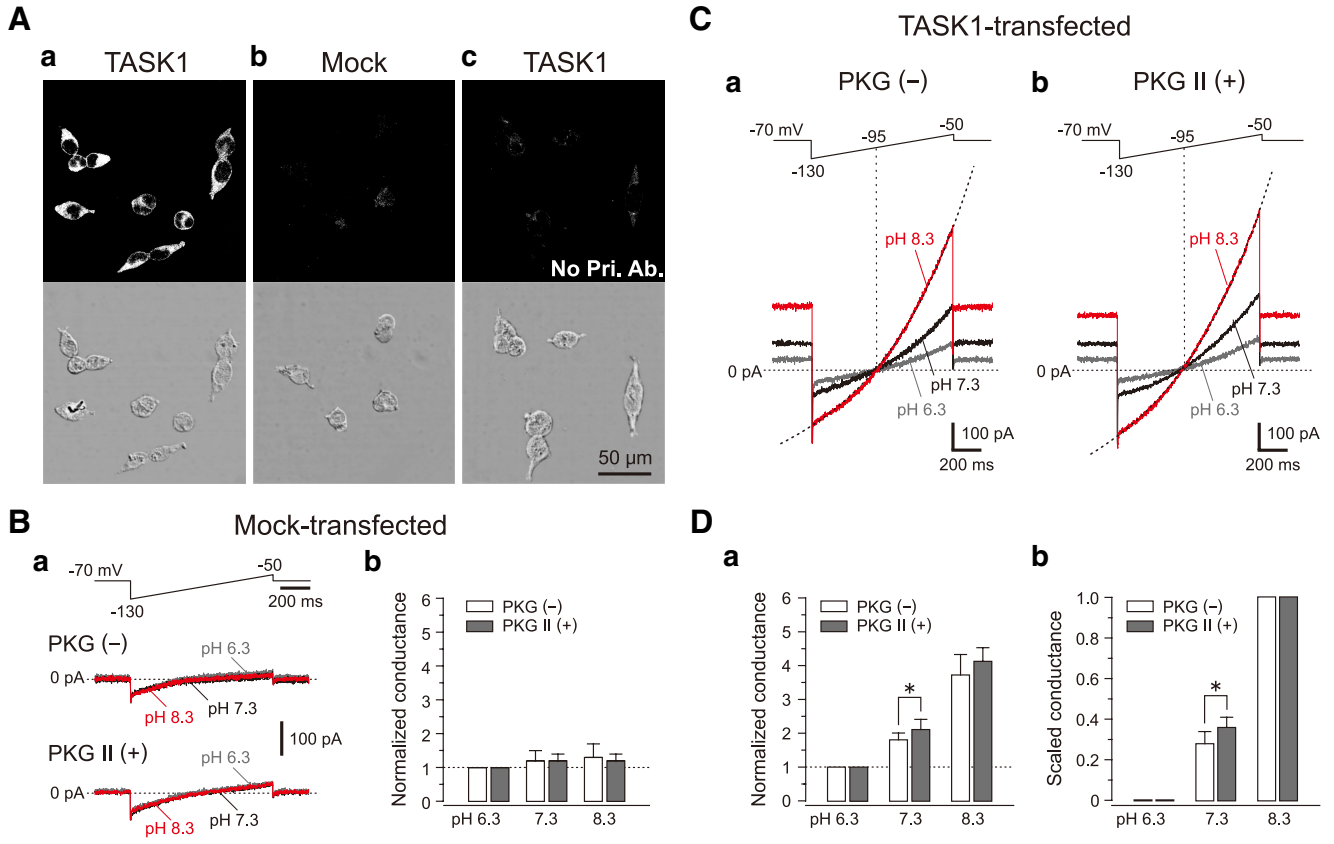

Figure 1. Modulation of TASK1 currents by basal level of PKG. ***A***, Photomicrographs of fluorescence images showing immunoreactivity for TASK1 channels (top) and bright-field images showing the presence of HEK cells in each experiment (bottom). The HEK cells transfected with TASK1 displaying unambiguous immunoreactivity along the plasma membrane and partly in the cytoplasm (***a***). The HEK cells transfected with mock displaying no intense immunoreactivity more than diffuse background fluorescence (***b***). The HEK cells transfected with TASK1 displaying no intense immunoreactivity in the absence of the primary antibody against TASK1 (***c***). ***Ba***, Top, Voltage command pulse. Bottom, Superimposed traces of small inwardly rectifying current responses obtained at pH 6.3, 7.3, and 8.3 in the PKG-unloaded and PKGII-loaded mock-transfected HEK cells. Note no apparent pH-sensitive K^+ current. ***Bb***, In the PKG-unloaded (open columns, $n = 5$) and PKGII-loaded (gray columns, $n = 8$) mock-transfected HEK cells, the mean conductances normalized to those at pH 6.3 in the current responses obtained at pH 6.3 (1.0 and 1.0, respectively), at pH 7.3 (1.2 ± 0.3 and 1.2 ± 0.2, respectively), and at pH 8.3 (1.3 ± 0.4 and 1.2 ± 0.2, respectively). ***C***, Top, Voltage command pulses. Bottom, Sample current traces obtained at pH 6.3, 7.3, and 8.3 in TASK1-transfected HEK cells in the absence (***a***) and presence (***b***) of PKGII. Black dotted curves obtained by fitting the TASK1 currents at pH 8.3 (red traces) with GHK equation. ***D***, Pooled data showing the mean values of normalized conductances (***a***) and the mean values of scaled conductances (***b***) at pH 6.3, 7.3, and 8.3 in the absence (open columns, $n = 5$) and presence (gray columns, $n = 6$) of PKGII. *$p < 0.05$ (‡).

loaded HEK cells, application of 100 μM 8-Br-cGMP clearly increased the TASK1 current at pH 7.3 (Fig. 2*Ba*,*Bb*, compare **2* and **3*). The mean value of conductance increases in TASK1 channels caused by application of 8-Br-cGMP at pH 7.3 ($(G_{7.3}^{8\text{-Br}} - G_{7.3})/G_{7.3}$) in the PKGII-loaded HEK cells (51 ± 12%, $n = 5$) was significantly (‡) larger than that obtained in the PKG-unloaded ones (13 ± 9%, $n = 6$) and also significantly (‡) larger than that in the heat-inactivated PKGII-loaded ones (15 ± 6%, $n = 8$) (Fig. 2*C*, gray columns). The mean values of conductance increases at pH 7.3 in the PKG-unloaded and PKGII-loaded mock-transfected HEK cells were only 2 ± 2% ($n = 6$) and 2 ± 2% ($n = 8$), respectively (Fig. 2*C*, open columns). This suggests that 8-Br-cGMP had nearly no effect on the intrinsic channel activity of HEK cells, regardless of whether PKGII was included in the pipette solution or not, and also suggests that the intrinsic HEK channels were not involved in the enhancement of the conductance induced by 8-Br-cGMP application.

In the PKGII-loaded HEK cells (Fig. 2*B*), the pH decrease from 7.3 to 6.3 in the presence of 8-Br-cGMP markedly reduced the TASK1 current (Fig. 2*Ba*,*Bb*, compare **3* and **4*). There was no apparent difference in the amplitude between the TASK1 current at pH 6.3 obtained before and that during 8-Br-cGMP application (Fig. 2*Ba*,*Bb*, compare **1* and **4*). Following the pH increase from 6.3 to 8.3 in the presence of 8-Br-cGMP, the TASK1 current markedly increased in amplitude (Fig. 2*Ba*,*Bb*, compare **4* and **5*). Nevertheless, in the presence of 8-Br-cGMP, the TASK1 current obtained at pH 8.3 was only slightly larger than that obtained at pH 7.3 (Fig. 2*Ba*,*Bb*, compare **3* and **5*), in contrast to the substantial difference in the amplitude between the TASK1 current at pH 8.3 and that at pH 7.3 in the absence of 8-Br-cGMP (Fig. 1*Cb*). Effects of 8-Br-cGMP on TASK1 channels at pH 8.3 were separately examined in different HEK cells. In contrast to the case at pH 7.3, the TASK1 current at pH 8.3 was not significantly (†, $n = 5$) affected by 8-Br-cGMP application (Fig. 2*Bc*), as was the case at pH 6.3. As revealed by the pooled data analysis ($n = 5$), the mean conductance increases at pH 6.8 (21 ± 6%), pH 7.3 (51 ± 12%), and pH 7.8 (20 ± 5%) caused by 8-Br-cGMP in the PKGII-loaded HEK cells were significant (†), whereas those at pH 6.3 (3 ± 3%) and pH 8.3 (7 ± 5%) were not significant (†) (Fig. 2*Da*). This result suggests either that the effects of 8-Br-cGMP on TASK1 currents are dependent on external pH (see Discussion), or that 8-Br-cGMP changed the pH sensitivity of TASK1 currents. In the PKGII-loaded mock-transfected HEK cells ($n = 8$), the mean conductance increases caused by 8-Br-cGMP at pH 6.3 (2 ± 1%), pH 7.3 (2 ± 2%), and pH 8.3 (2 ± 2%) were not significant (†) (figure not shown),

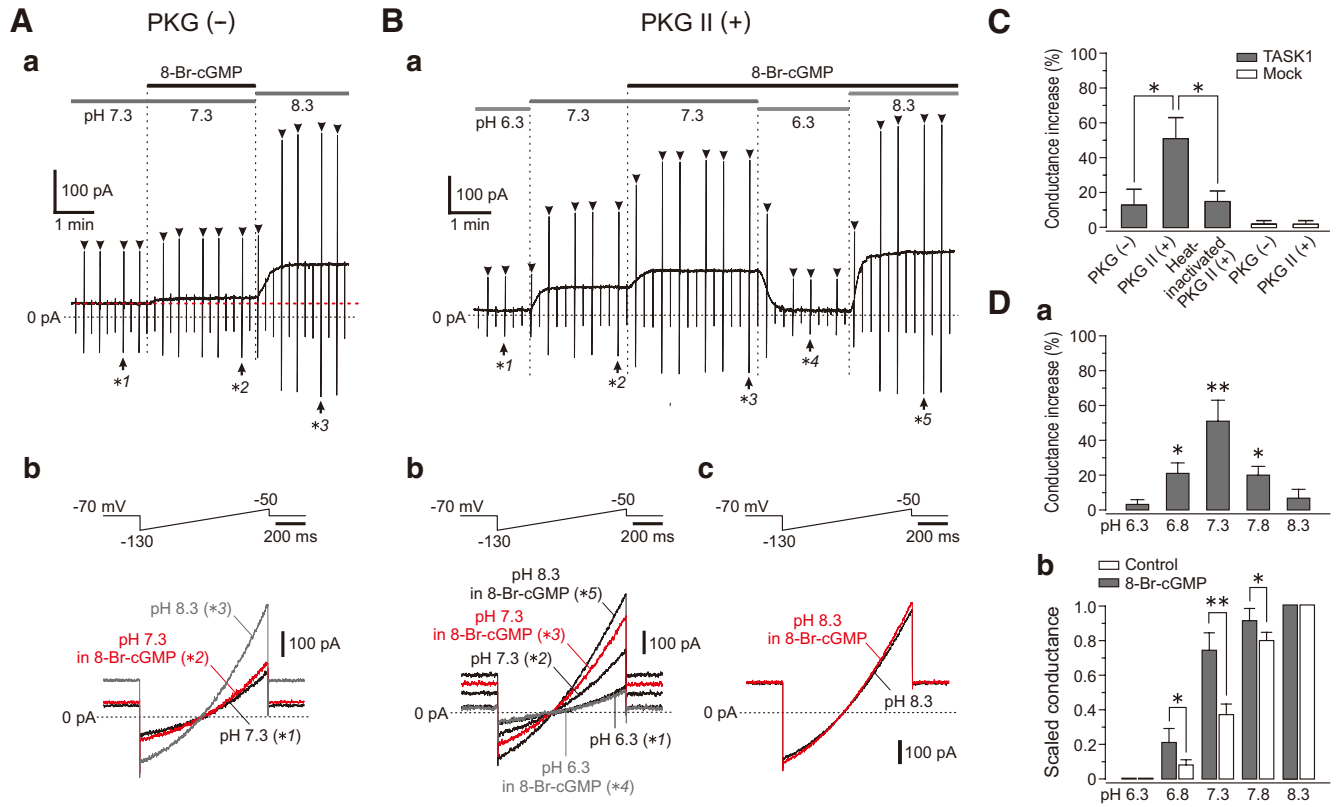

Figure 2. pH-dependent effects of 8-Br-cGMP on TASK1 currents. ***Aa***, ***Ba***, Sample traces of continuous recordings of TASK1 currents evoked in a PKG-unloaded HEK cell (***Aa***) and in a PKGII-loaded HEK cell (***Ba***) in response to repetitive application of step-and-ramp pulses at various pHs before and during application of 8-Br-cGMP. Gray and black horizontal bars represent the duration and timing of perfusion with respective pH solutions and those of 100 μM 8-Br-cGMP application, respectively. Arrowheads indicate the peak levels of current responses to the ramp pulse. The respective maximum amplitudes of current responses measured from the zero to the peak current level reflect the respective conductances. ***Ab***, ***Bb***, Top, Voltage command pulses. Bottom, superimposed current traces obtained at the time points indicated with **1*, **2*, and **3* in ***Aa*** and with **1*, **2*, **3*, **4*, and **5* in ***Ba***. ***Bc***, Top, Voltage command pulse. Bottom, Superimposed current traces obtained at pH 8.3 before and during application of 8-Br-cGMP in a different HEK cell. ***C***, Pooled data showing the mean conductance increases (%) in PKG-unloaded TASK1-transfected HEK cells ($n = 6$), PKGII-loaded TASK1-transfected HEK cells ($n = 5$), heat-inactivated PKGII-loaded TASK1-transfected HEK cells ($n = 8$), PKG-unloaded mock-transfected HEK cells ($n = 6$) and PKGII-loaded mock-transfected HEK cells ($n = 8$) following application of 8-Br-cGMP. *$p < 0.005$ (‡). ***Da***, Pooled data ($n = 5$) showing the mean conductance increases (%) following application of 8-Br-cGMP at pH 6.3, 6.8, 7.3, 7.8, and 8.3 in PKGII-loaded TASK1-transfected HEK cells. *$p < 0.002$, **$p < 0.001$ (†). ***Db***, Pooled data ($n = 5$) showing the mean values of scaled conductances in the presence (gray columns) and absence (open columns) of 8-Br-cGMP in PKGII-loaded TASK1-transfected HEK cells. (S-$G_x^{8\text{-Br}}$ vs S-G_x) at pH 6.3, 6.8, 7.3, 7.8, and 8.3 were (0 vs 0), (0.21 ± 0.08 vs 0.08 ± 0.03), (0.74 ± 0.10 vs 0.37 ± 0.06), (0.91 ± 0.07 vs 0.80 ± 0.05), and (1 vs 1), respectively. *$p < 0.05$, **$p < 0.001$ (§, *post hoc*).

suggesting that the intrinsic HEK channels were not responsible for the effects of 8-Br-cGMP on the pH sensitivity of TASK1 currents.

To examine whether the pH sensitivity is different between the TASK1 currents obtained before and during application of 8-Br-cGMP or not, the TASK1 currents obtained at various pHs in the absence and presence of 8-Br-cGMP were represented as the scaled conductances (S-G_x and S-$G_x^{8\text{-Br}}$, respectively) and were compared. There was a significant (§) difference between the pH profiles of the scaled conductances obtained before and during 8-Br-cGMP application (Fig. 2*Db*, open columns vs gray columns). The pH profile appeared to be shifted in the acidic direction by 8-Br-cGMP application. Therefore, it is strongly suggested that activation of PKGII by 8-Br-cGMP upregulates TASK1 currents significantly at pH 6.8, 7.3, and 7.8 (§, *post hoc*) by shifting the pH sensitivity profile in the acidic direction. Furthermore, PKGIα was also effective for the activation of TASK1 currents. Similar to that obtained in the PKGII-loaded HEK cells, the mean conductance increase after application of 8-Br-cGMP at pH 7.3 in the PKGIα-loaded HEK ones was 41 ± 8% ($n = 6$, figure not shown), although the effects of 8-Br-cGMP were not examined at pHs except 7.3. Thus, both subtypes of PKG were effective for the activation of TASK1 currents.

KT5823 facilitates pH-dependent inhibition of TASK1 currents in PKGII-loaded HEK cells

If PKG activation by 8-Br-cGMP really shifts the pH sensitivity profile of TASK1 currents in the acidic direction, PKG inhibition is expected to shift the pH sensitivity profile in the basic direction. This possibility was examined by using a PKG inhibitor, KT5823. Bath application of 2 μM KT5823 at pH 7.3 apparently reduced the TASK1 currents at pH 7.3 (Fig. 3*Aa*,*Ab*, compare **1* and **2*). Thereafter, in the presence of KT5823, the TASK1 currents remained almost unchanged, regardless of the pH decrease from 7.3 to 6.3 (Fig. 3*Aa*,*Ab*, compare **2* with **3* and **4*). In contrast, when the pH was increased from 6.3 to 7.8 and 8.3 in the presence of KT5823, the TASK1 currents remarkably increased (Fig. 3*Aa*,*Ab*, **5* and **6*). These changes in the TASK1 currents could be more clearly seen in the changes in the conductance, which is reflected in the peak level (Fig. 3*Aa*, arrowheads) of current responses to the ramp pulse when referred to the zero current level. However, at pH 8.3, the TASK1 current was not significantly (†, $n = 5$) affected by KT5823 (figure not shown), similar to the case with 8-Br-cGMP (Fig. 2*Bc*). There was a significant (§) difference between the pH profiles of the scaled conductances obtained before and during KT5823 application (Fig. 3*Ac*, open and gray columns, respectively). The pH pro-

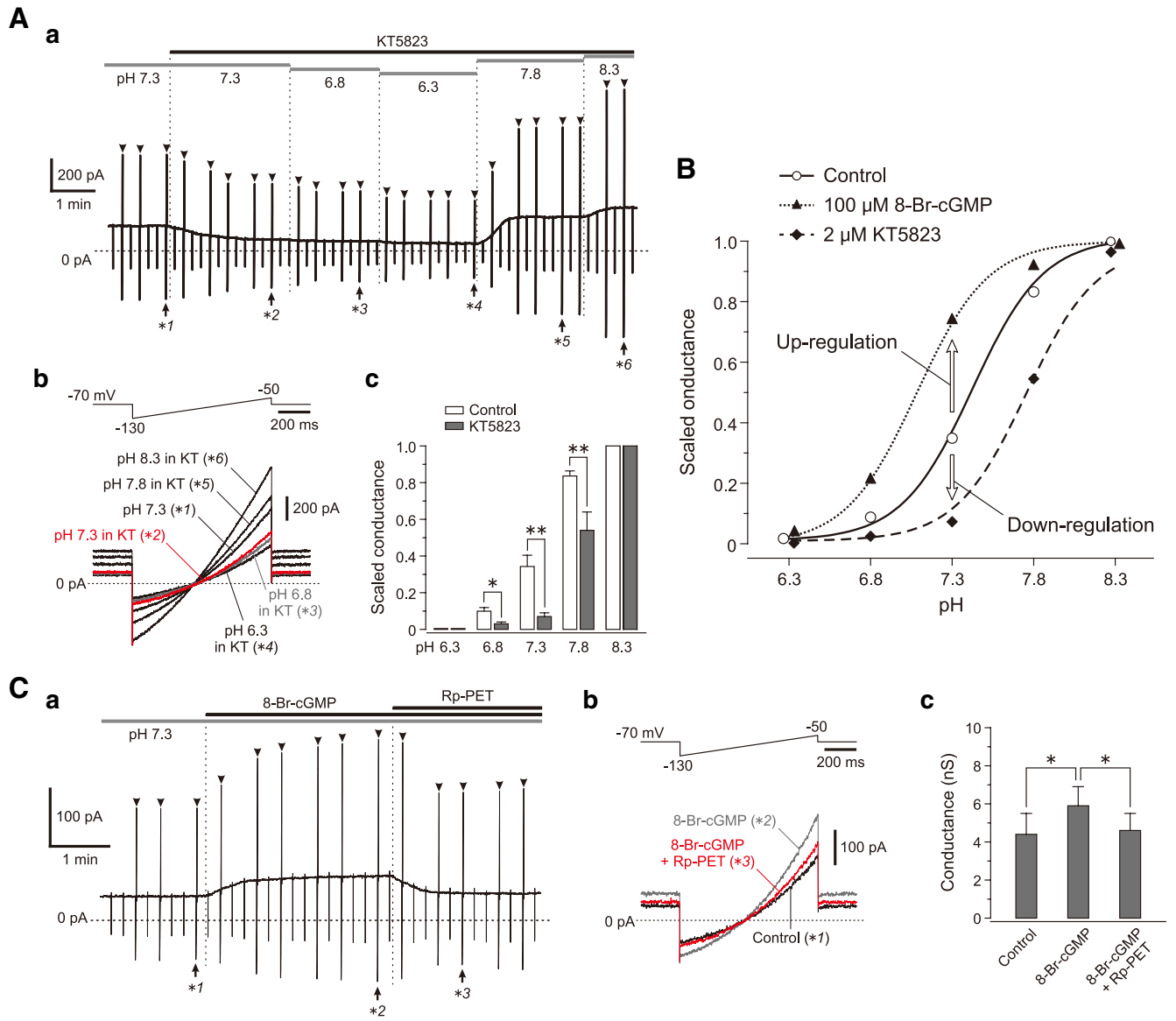

Figure 3. Inhibition of TASK1 currents by KT5823 in a pH-dependent manner. ***Aa***, A sample trace of a continuous recording of TASK1 currents obtained in a PKGII-loaded HEK cell in response to repetitive application of step-and-ramp pulses at various pHs before and during application of 2 μM KT5823. Gray and black horizontal bars indicate the duration and timing of perfusion with respective pH solutions and those of KT5823 application, respectively. Arrowheads indicate the peak levels of current responses to the ramp pulse, reflecting the respective conductances. ***Ab***, Top, Voltage command pulse. Bottom, Superimposed current traces obtained at the time points indicated with **1*, **2*, **3*, **4*, **5*, and **6* in ***Aa***. ***Ac***, Pooled data ($n = 5$) showing the mean values of scaled conductances in the absence (open columns) and presence (gray columns) of KT5823 at pH 6.3, 6.8, 7.3, 7.8, and 8.3. (S-G_x vs S-G_x^{KT}) at pH 6.3, 6.8, 7.3, 7.8, and 8.3 were (0 vs 0), (0.10 $\pm$ 0.02 vs 0.03 $\pm$ 0.01), (0.34 $\pm$ 0.07 vs 0.07 $\pm$ 0.02), (0.83 $\pm$ 0.04 vs 0.54 $\pm$ 0.10), and (1 vs 1), respectively. *$p < 0.05$, **$p < 0.001$ (§, *post hoc*). ***B***, Bidirectional modulation of the pH profile of scaled conductances. The interrupted, continuous, and dotted curves obtained with the Hill equation by fitting the respective pH profiles of scale conductances in the presence of KT5823 (filled diamonds), in the control condition (open circles) and in the presence of 8-Br-cGMP (filled triangles). Hill coefficient, 2. ***Ca***, A sample trace of a continuous recording of TASK1 currents evoked in a PKGII-loaded HEK cell in response to repetitively applied step-and-ramp pulses at pH 7.3. Long and short black horizontal bars indicate the duration and timing of 100 μM 8-Br-cGMP and those of 20 μM Rp-PET application, respectively. Arrowheads indicate the peak levels of current responses to the ramp pulse, reflecting the respective conductances. ***Cb***, Top, Voltage command pulse. Bottom, Superimposed current traces obtained at the time points indicated with **1*, **2*, and **3* in ***Ca***. ***Cc***, The mean conductances ($n = 6$) obtained before and during application of 8-Br-cGMP and during coapplication of 8-Br-cGMP and Rp-PET at pH 7.3. *$p < 0.001$ (§, *post hoc*).

file appeared to be shifted in the basic direction by KT5823 application. Therefore, it is strongly suggested that KT5823 facilitated the pH-dependent inhibition of the TASK1 currents significantly at pH 6.8, 7.3, and 7.8 (§, *post hoc*) by shifting the pH sensitivity profile in the basic direction. Together, it is likely that PKG activation and inhibition can respectively upregulate and downregulate the TASK1 current at physiological pH by shifting its pH sensitivity profile in the acidic and basic directions, respectively (Fig. 3*B*).

Modulation of TASK1 currents depending on the level of PKG activity

To directly verify that under the physiological pH the TASK1 current is modulated by a level of PKG activity, we next examined whether the enhancement of the TASK1 currents by 8-Br-cGMP is reversed by a competitive PKG inhibitor, Rp-PET. At pH 7.3, application of 100 μM 8-Br-cGMP significantly (§, *post hoc*) increased the mean conductance from 4.4 $\pm$ 1.1 to 5.9 $\pm$ 1.0 nS ($n = 6$) (Fig. 3*Ca*,*Cb*, compare **1* and **2*; see also Fig. 3*Cc*), which

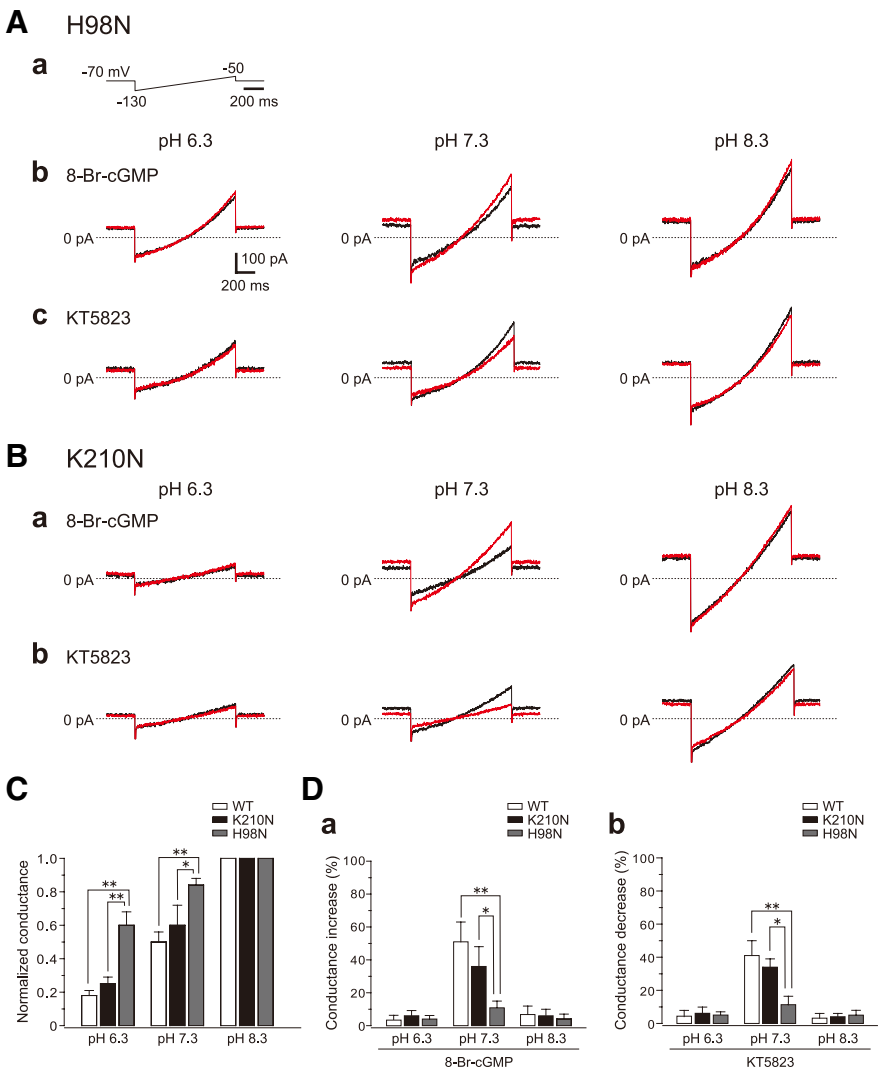

Figure 4. Effects of 8-Br-cGMP and KT5823 on TASK1 mutants H98N and K210N. ***A***, Voltage command pulse (***a***). Superimposed traces of current responses obtained at pH 6.3, 7.3, and 8.3 in H98N channels in the absence (black traces) and presence (red traces) of 8-Br-cGMP (***b***) or KT5823 (***c***). Sample current traces at pH 8.3 were obtained from different HEK cells in ***b*** and ***c***. Calibration bars for time scale and current amplitude shown in ***b*** also apply to all other current responses in ***A*** and ***B***. ***B***, Superimposed traces of current responses obtained at pH 6.3, 7.3, and 8.3 in K210N channels in the absence (black traces) and presence (red traces) of 8-Br-cGMP (***a***) or KT5823 (***b***). ***C***, Pooled data showing the mean conductance normalized to that at pH 8.3 in the current responses obtained at pH 6.3, at pH 7.3 and at pH 8.3 in WT TASK1 channels (open columns, $n = 7$), K210N channels (black columns, $n = 6$) and H98N channels (gray columns, $n = 5$). $^*p < 0.05$, $^{**}p < 0.005$ (§, *post hoc*). ***D***, Pooled data showing percentage increases (***a***)/decreases (***b***) of the mean conductance following application of 8-Br-cGMP/KT5823 in WT TASK1 channels (open columns, $n = 5/5$), K210N channels (black columns, $n = 4/5$) and H98N channels (gray columns, $n = 5/7$) at respective pHs. $^*p < 0.05$, $^{**}p < 0.005$ (§, *post hoc*).

were promptly and significantly (§, *post hoc*) reduced by the subsequent coapplication of 20 μM Rp-PET and 8-Br-cGMP to 4.6 ± 0.9 nS (Fig. 3*Ca*,*Cb*, compare **2* and **3*; see also Fig. 3*Cc*). These results indicate that TASK1 currents around the physiological pH can be dynamically modulated by the level of PKG activity.

Together, it can be hypothesized that PKG affected the pH sensors of TASK1 channels to change their pH sensitivities. In the next experiments, we directly addressed this possibility by using TASK1 mutants, in which the extracellular pH sensors, H98 and K210, were mutated.

Effects of PKG modulators on TASK1 mutants H98N and K210N

To clarify whether the pH sensor is directly involved in the modulation of TASK1 channels by PKG activation/inhibition or not, we examined the effects of PKG modulators on TASK1 channels with mutations of H98 and K210 to asparagine (H98N and K210N, respectively), in which the pH sensitivity in the physiological pH range was largely abolished or decreased as reflected in smaller Hill coefficients and larger K_d in comparison with WT (Morton et al., 2003).

First, the pH sensitivities of TASK1 mutant channels H98N and K210N were verified in PKGII-loaded HEK cells. The pH profiles of H98N and K210N channels can be illustrated from sample current traces obtained in response to the ramp pulse at pH 6.3, 7.3, and 8.3, shown as controls for PKG modulations in Figure 4, *A* and *B* (black traces), respectively. As revealed by the pooled data analysis, the mean values of respective conductances at pH 6.3 and 7.3, normalized to that at pH 8.3 in H98N channels (0.60 ± 0.08 and 0.84 ± 0.04, respectively, $n = 5$) were significantly (§, *post hoc*) larger than those obtained in WT channels (0.18 ± 0.03 and 0.50 ± 0.06, respectively, $n = 7$) and also significantly (§, *post hoc*) larger than those in K210N channels (0.25 ± 0.04 and 0.60 ± 0.12, respectively, $n = 6$) (Fig. 4*C*). The mean values of conductances at pH 6.3 and 7.3, normalized to that at pH 8.3 in K210N channels were slightly but insignificantly (§, *post hoc*) larger than those obtained at pH 6.3 and 7.3 in WT channels (Fig. 4*C*). These results indicate that the rank of the pH sensitivity in ascending order was: H98N < K210N ≤ WT, consistent with the previous report (Morton et al., 2003).

Then, the effects of 8-Br-cGMP/KT5823 were examined on H98N and K210N channels. In H98N channels, an application of 100 μM 8-Br-cGMP/2 μM KT5823 at pH 7.3 slightly increased/decreased the current response (Fig. 4*A*, compare black and red traces), while in K210N channels considerably increasing/decreasing the current response (Fig. 4*B*, compare black and red traces). However, the current responses at pH 6.3 and 8.3 were not markedly affected by 8-Br-cGMP/KT5823 application both in H98N and K210N channels (Fig. 4*A*,*B*, compare black and red traces).

As revealed by the pooled data analysis, the mean values of conductance increases/decreases caused by application of 8-Br-cGMP/KT5823 at pH 7.3 in H98N channels (11 ± 4%, $n = 5$)/(13 ± 6%, $n = 7$) were significantly (§, *post hoc*) smaller than those obtained in WT channels (51 ± 12%, $n = 5$)/(41 ± 9%, $n = 5$) and also significantly (§, *post hoc*) smaller than those in K210N channels (36 ± 12%, $n = 4$)/(34 ± 5%, $n = 5$) (Fig. 4*D*). The mean conductance increases/decreases at pH 7.3 caused by 8-Br-GMP/KT5823 in K210N channels were smaller than those in WT channels, although there were no significant (§, *post hoc*) differences between them (Fig. 4*D*).

Thus, the rank order of the enhancement/inhibition of current responses by 8-Br-cGMP/KT5823 at pH 7.3 was as follows: WT ≥ K210N > H98N, which is the same as that of their Hill coefficients. These results indicate that the PKG modulation of the current responses was largely abolished or decreased by mutations of the pH sensors in a manner inversely proportional to the potency of protonation of mutated pH sensor, suggesting that the modulatory effects of PKG are mediated by the activity of the pH sensors. Therefore, it is likely that PKG-mediated phosphorylation of an intracellular site on TASK1 channels alters the local environment of the pH sensors situated on the two pore loops of TASK1 channels to change K_d values for protonation of pH sensors.

In the following series of experiments, we examined whether and how PKG modulates the pH sensitivity of I-K_{leak} in cholinergic BF neurons.

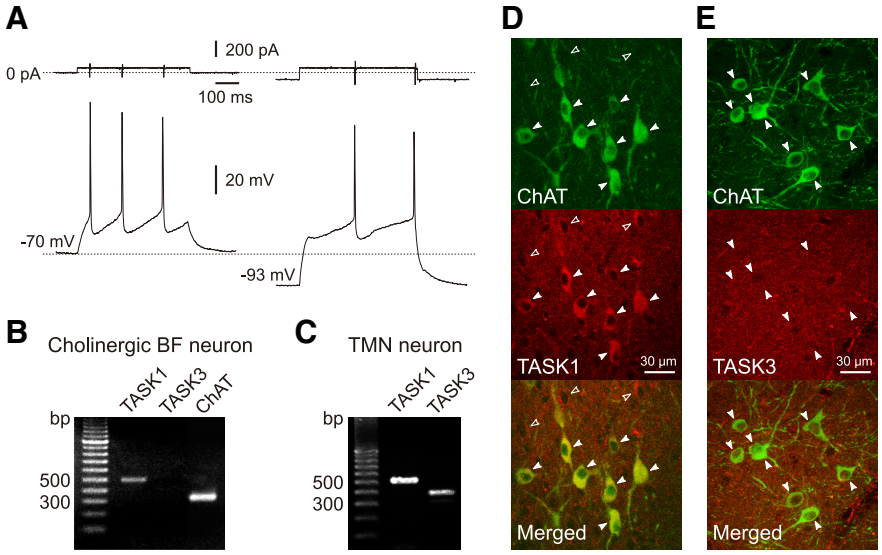

Figure 5. Expression of TASK1, TASK3, and ChAT in MS/DB neurons. ***A***, A type II neuron displaying either a late spiking due to A-like K^+ current in response to a depolarizing current pulse applied at −93 mV (right) or a regular spiking at −70 mV (left). ***B***, mRNA expression profile of TASK1, TASK3, and ChAT obtained from the type II neuron shown in ***A***, revealed by single-cell RT-PCR. Note that TASK1 mRNA was expressed together with ChAT mRNA in the type II neuron. ***C***, mRNA expression profile of TASK1 and TASK3 obtained from a TMN neuron. The amplified PCR fragments were consistent with the respective lengths predicted by the two subunit primers. ***D***, ***E***, Confocal photomicrographs showing immunoreactivity for ChAT (green) and TASK1 or TASK3 (red) in neurons of MS/DB nuclei. As revealed in the merged images, both cholinergic neurons (filled arrowheads) and noncholinergic neurons (open arrowheads) were immunopositive for TASK1 antibody (***D***), while neither cholinergic (filled arrowheads) nor noncholinergic neurons were immunopositive for TASK3 antibody (***E***).

Expression of TASK channels in cholinergic BF neurons

First, we investigated whether TASK1 and/or TASK3 channels are expressed together with ChAT in the presumed cholinergic BF neurons, by using a single-cell RT-PCR method. We previously presumed the type II neuron as cholinergic (Kang et al., 2007), based on its late-spiking pattern due to A-like K^+ current in response to depolarizing current pulses applied at a hyperpolarized holding potential (Fig. 5*A*), which is characteristic to cholinergic BF neurons (Griffith and Matthews, 1986; Markram and Segal, 1990; Sim and Allen, 1998). By performing single-cell RT-PCR on identified type II neurons (Fig. 5*A*), both TASK1 and ChAT mRNAs were found to be simultaneously expressed in all of 14 type II neurons examined, whereas TASK3 mRNA was observed in none of those type II neurons (Fig. 5*B*), in contrast to motoneurons of the TMN used as positive controls for detecting TASK1/3 mRNAs (Fig. 5*C*).

Consistent with these observations, virtually all ChAT-positive (cholinergic) neurons in the BF displayed TASK1 immunoreactivity (Fig. 5*D*, filled arrowheads), while some of the ChAT-negative (noncholinergic) neurons were also immunoreactive to TASK1 (Fig. 5*D*, open arrowheads). The absorption test and negative control for the TASK1 immunoreactivity were presented in supplemental Fig. 1, *A* and *B*, available at www.jneurosci.org as supplemental material. In contrast, ChAT-positive neurons in the BF exhibited very weak or no immunoreactivity for TASK3 (Fig. 5*E*, filled arrowheads). A positive control for the TASK3 immunoreactivity was presented in supplemental Fig. 1*C*, available at www.jneurosci.org as supplemental material.

Since the coexistence of TASK1 and ChAT mRNAs was detected in type II neurons in the single-cell RT-PCR method and since TASK1 channels were expressed in cholinergic MS/DB neurons as revealed in the immunohistochemical method, type II neurons recorded from MS/DB nuclei can be identified as cholinergic BF neurons that express TASK1 channels. Therefore, the major component of the I-K_{leak} in type II neurons is likely to be mediated by TASK1 channels, as reflected in its pH sensitivity profile that was almost the same as that of TASK1 current (Toyoda et al., 2008).

KT5823 downregulates the I-K_{leak} at pH 7.3 in cholinergic BF neurons

Since PKG activation upregulated the I-K_{leak} at pH 7.3 in our previous study (Toyoda et al., 2008), we first examined whether the inhibition of PKG activity downregulates the I-K_{leak} at pH 7.3 or not. Following a decrease in pH from 8.3 to 7.3, the I-K_{leak} recorded in a cholinergic BF neuron was decreased gradually, as seen in the baseline current and in the current responses to the ramp pulses (Fig. 6*Aa*,*Ab*, **1*, **2*, and **3*). When 2 μM KT5823 was bath applied after the baseline current reached a steady level at pH 7.3, the baseline current and the outward component of the current response at pH 7.3 was markedly decreased (Fig. 6*Aa*,*Ab*, compare **3* and **4*). Thereafter, when the pH was decreased from 7.3 to 6.3 and 6.8 in the presence of KT5823, the current responses remained almost unchanged (Fig. 6*Aa*,*Ad*, compare **4* with **5* and **6*).

The *I–V* relationship of the KT5823-sensitive current at pH 7.3 obtained by subtraction of **4* from **3* (Fig. 6*Ac*, **3* − **4*) displayed the GHK outward rectification (Fig. 6*Ac*, red dotted curve), consistent with the nature of TASK currents (Goldstein et al., 2001; Patel and Honoré, 2001; Bayliss et al., 2003). In contrast, there was no pH-sensitive component following the pH changes from 7.3 to 6.3 and 6.8 in the presence of KT5823, as revealed by the *I–V* relationships obtained by subtraction of **5* from **4* and **5* from **6* (Fig. 6*Ae*, **4* − **5* and **6* − **5*). Thus, the inhibition of the possible intrinsic PKG activity by KT5823 decreased the TASK1-like I-K_{leak} at pH 7.3 and 6.8 to be as small as that at pH 6.3.

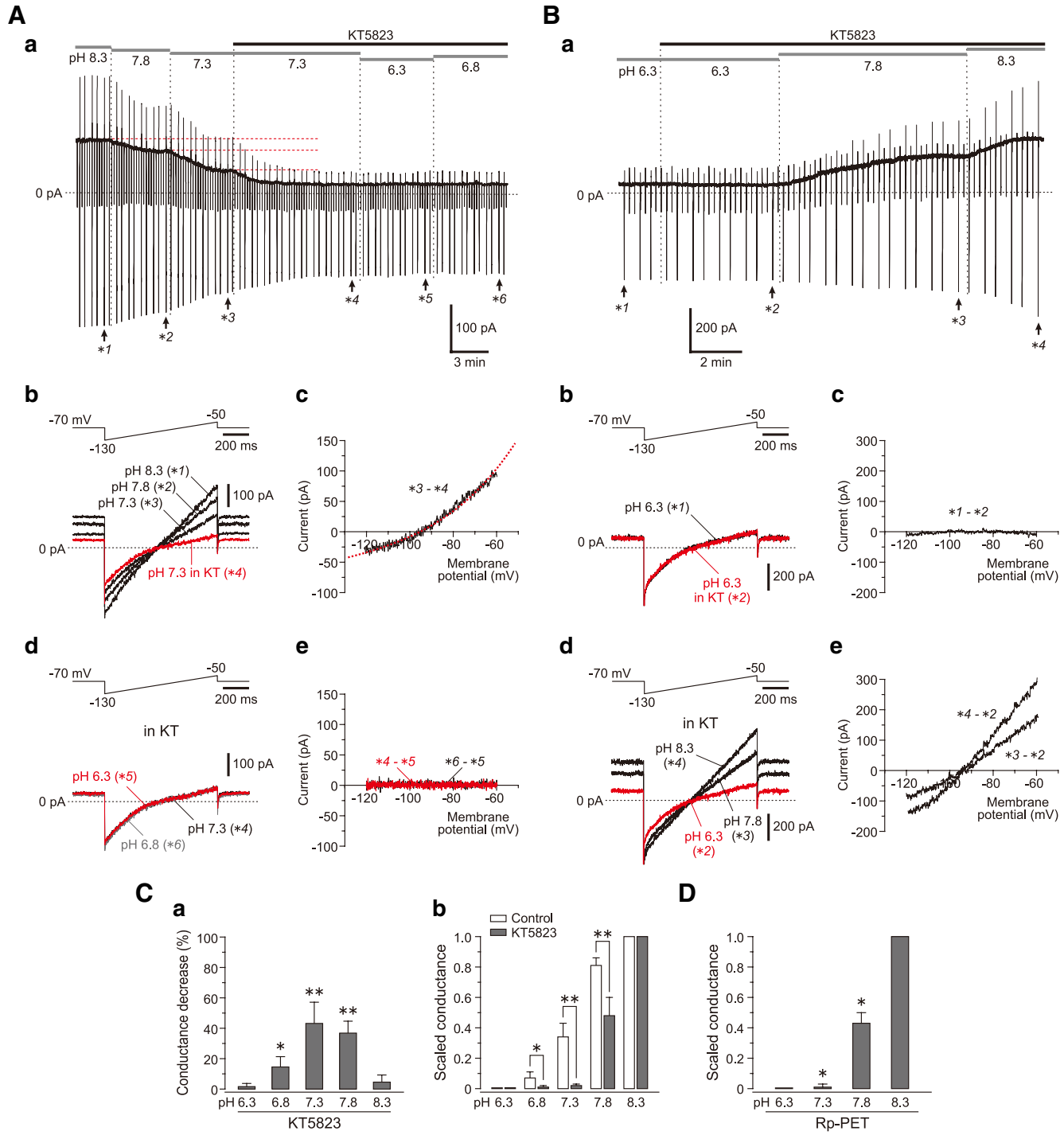

Figure 6. KT5823 and Rp-PET inhibit the I-K_{leak} in a pH-dependent manner. ***Aa***, A sample continuous recording of current responses obtained in a cholinergic BF neuron in response to repetitive application of step-and-ramp pulses at various pHs (gray horizontal bars) before and during application of 2 μM KT5823 (black horizontal bar). ***Ab***, ***Ad***, Top, Voltage command pulses. Bottom, Superimposed current traces obtained at the time points indicated with **1*, **2*, **3*, and **4* (***Ab***) and with **4*, **5*, and **6* (***Ad***) in ***Aa***. ***Ac***, ***Ae***, I–V relationship of KT5823-sensitive current at pH 7.3 (***Ac***, **3* − **4*) and those of pH-sensitive currents obtained following pH decrease from 7.3 to 6.3 (***Ae***, **4* − **5*) and from 6.8 to 6.3 (***Ae***, **6* − **5*) in the presence of KT5823. Red dotted curve obtained by fitting the I–V relationship of KT5823-sensitive current at pH 7.3 with GHK equation. ***Ba***, A sample continuous recording of current responses obtained in a cholinergic BF neuron in response to repetitive application of step-and-ramp pulses at various pHs (gray horizontal bars) before and during application of 2 μM KT5823 (black horizontal bar). ***Bb***, ***Bd***, Top, Voltage command pulses. Bottom, Superimposed current traces obtained at the time points indicated with **1* and **2* (***Bb***) and with **2*, **3*, and **4* (***Bd***) in ***Ba***. ***Bc***, ***Be***, I–V relationships of KT5823-sensitive current at pH 6.3 (***Bc***) and pH-sensitive K^+ currents in the presence of KT5823 (***Be***). Note no apparent KT5823-sensitive current at pH 6.3 examined at any potential from −120 to −60 mV (***Bc***, **1* − **2*). Note the emergence of prominent I-K_{leak} following pH increase from 6.3 (**2*) to 7.8 (**3*) or 8.3 (**4*) even in the presence of KT5823 (***Be***, **3* − **2* and **4* − **2*). ***Ca***, Pooled data showing the mean conductance decreases (%) following application of KT5823 at pH 6.3 ($n = 5$), 6.8 ($n = 6$), 7.3 ($n = 6$), 7.8 ($n = 7$), and 8.3 ($n = 5$). *$p < 0.05$, **$p < 0.005$ (†). ***Cb***, Open and gray columns represent the mean values of scaled conductances at pH 6.3, 6.8, 7.3, 7.8, and 8.3 in the absence (S-G_x, open columns) and presence (S-G_x^{KT}, gray columns) of KT5823. (S-G_x vs S-G_x^{KT}) at pH 6.3, 6.8, 7.3, 7.8, and 8.3 were (0 vs 0), (0.07 ± 0.04 vs 0.01 ± 0.01), (0.34 ± 0.09 vs 0.02 ± 0.01), (0.81 ± 0.05 vs 0.47 ± 0.12), and (1 vs 1), respectively. *$p < 0.05$, **$p < 0.001$ (§, *post hoc*). ***D***, The mean values of scaled conductances at pH 6.3 ($n = 6$), 7.3 ($n = 6$), 7.8 ($n = 6$), and 8.3 ($n = 6$) in the presence of 10 μM Rp-PET. *$p < 0.001$ (vs control; ‡).

KT5823 facilitates the pH-dependent inhibition of the *I*-K_{leak}

Effects of 2 μM KT5823 on the *I*-K_{leak} at a basic pH range were separately examined in a different cholinergic BF neuron (Fig. 6*Ba*). At first, it was confirmed that KT5823 does not decrease the *I*-K_{leak} at pH 6.3 (Fig. 6*Ba*,*Bb*, compare **1* and **2*). As revealed by the *I–V* relationship obtained by subtraction of **2* from **1* (Fig. 6*Bc*, **1* − **2*), there was nearly no difference in the current response at pH 6.3 obtained before and during application of KT5823. However, when the pH was increased from 6.3 to 7.8 and 8.3 in the presence of KT5823, the current responses markedly increased (Fig. 6*Ba*,*Bd*, compare **2* with **3* and **4*), as revealed by large pH-sensitive currents obtained by subtraction of **2* from **3* and from **4* (Fig. 6*Be*, **3* − **2* and **4* − **2*).

As revealed by the pooled data analysis, there were significant (†) decreases in the mean conductances only at pH 6.8, 7.3, and 7.8 following application of KT5823 (Fig. 6*Ca*). This result suggests either that the effects of KT5823 on the *I*-K_{leak} are dependent on external pH (see Discussion), or that KT5823 changed the TASK1-like pH sensitivity of the *I*-K_{leak}. There was a significant (§) difference in the pH profile between the scaled conductances obtained before and during KT5823 application (Fig. 6*Cb*, open columns vs gray columns). These results would indicate that KT5823 facilitated the pH-dependent inhibition of the *I*-K_{leak} significantly at pH 6.8, 7.3, and 7.8 (§, *post hoc*) by changing the pH sensitivity, consistent with the results obtained from HEK cells (Fig. 3*A*).

Similar findings were also obtained by using Rp-PET, another PKG inhibitor (Fig. 6*D*, figure not shown). In comparison with the control scaled conductances for KT5823 (Fig. 6*Cb*, open columns), the pH profile of the scaled conductances in the presence of 10 μM Rp-PET was significantly (‡) different (Fig. 6*D*). These results would indicate that KT5823 and Rp-PET markedly suppressed the removal of the pH-dependent inhibition of the *I*-K_{leak} following pH increase to 7.3, while suppressing much less markedly following pH increase to 7.8 and 8.3, presumably changing its pH sensitivity. However, it is yet unclear whether the *I*-K_{leak} remained partly inhibited by KT5823/Rp-PET even at pH 8.3 or not. This question was addressed in the next experiment.

Rp-PET does not inhibit the *I*-K_{leak} at pH 8.3

In the presence of 10 μM Rp-PET, the current response was increased following pH increase from 7.3 to 8.3 (Fig. 7*Aa*). However, the current response at pH 8.3 in the presence of 10 μM Rp-PET (Fig. 7*Aa*,*Ab*, **1*) was hardly increased by the washout of Rp-PET for 4 min and by the subsequent application of 200 μM 8-Br-cGMP (Fig. 7*Aa*,*Ab*, **2*), as revealed by subtraction of **1* from **2* (Fig. 7*Ac*, **2* − **1*). Since 8-Br-cGMP and Rp-PET competitively act on the cGMP-binding site of PKG (Butt et al., 1992, 1995), the 8-Br-cGMP application would have increased the current response if Rp-PET markedly suppressed the current response at pH 8.3. There was no significant (†) difference in the mean conductance ($n = 6$) between the current responses recorded at pH 8.3 in the presence of Rp-PET and those recorded at pH8.3 following application of 8-Br-cGMP after a brief washout of Rp-PET (Fig. 7*Ad*). This result would indicate that Rp-PET did not suppress the removal of the pH-dependent inhibition of the *I*-K_{leak} following the pH increase to 8.3 but rather allowed it completely.

Thus, it was demonstrated that the inhibition of PKG activity by KT5823 and Rp-PET depressed the *I*-K_{leak} at pH 7.3 and 6.8 as small as that caused following pH decrease to 6.3, but did much less markedly at pH 7.8 and almost not at all at pH 8.3, by causing a shift in the TASK1-like pH sensitivity profile of the *I*-K_{leak} in the basic direction, consistent with the results obtained from HEK cells (Fig. 3*A*).

Rp-PET reverses 8-Br-cGMP-induced currents

To further verify that under the physiological pH the *I*-K_{leak} is modulated by the level of PKG activity, it was examined whether the enhancement of the *I*-K_{leak} by 8-Br-cGMP is reversed by Rp-PET or not. An application of 200 μM 8-Br-cGMP markedly increased both the baseline current and the conductance (Fig. 7*Ba*,*Bb*, compare **1* and **2*), which were transiently reversed almost to the control level by the subsequent coapplication of 20 μM Rp-PET and 8-Br-cGMP (Fig. 7*Ba*, compare **2* and **3*). The *I–V* relationship of the Rp-PET-sensitive current obtained by subtraction of **3* from **2* (Fig. 7*Bc*, **2* − **3*) was almost the same as that of the 8-Br-cGMP-induced current obtained by subtraction of **1* from **2* (Fig. 7*Bc*, **2* − **1*), revealing the almost complete inhibitory effect of Rp-PET on the 8-Br-cGMP-induced conductance. Following simultaneous washout of Rp-PET and 8-Br-cGMP, both the baseline current and the conductance increased and slightly exceeded their values obtained just before the coapplication of Rp-PET with 8-Br-cGMP (Fig. 7*Ba*, **4*).

The mean conductance examined at pH 7.3 ($n = 6$) was significantly (§, *post hoc*) increased from 3.0 ± 1.3 to 6.9 ± 1.9 nS following application of 8-Br-cGMP, but was significantly (§, *post hoc*) decreased to 3.1 ± 1.2 nS by the subsequent coapplication of Rp-PET and 8-Br-cGMP (Fig. 7*Bd*). These observations strongly suggest that under the physiological pH the *I*-K_{leak} can be modulated by the balance between 8-Br-cGMP and Rp-PET, i.e., by the level of PKG activity (see supplemental information and supplemental Fig. 2, available at www.jneurosci.org as supplemental material), consistent with the observation made in PKGII-loaded HEK cells expressing TASK1 (Fig. 3*C*).

Discussion

Comparison of PKG activity between HEK cells and cholinergic BF neurons

The present study demonstrated for the first time that activation and inhibition of PKG respectively upregulate and downregulate recombinant TASK1 channels heterologously expressed in PKG-loaded HEK cells. In the presence of 8-Br-cGMP, the scaled conductance around pH 7.3 in HEK cells was smaller than that in cholinergic BF neurons observed in our previous study (Toyoda et al., 2008) (Fig. 8, compare dotted curves in *A*,*B*). This may be because the action of exogenously applied PKG in the HEK cells in response to 8-Br-cGMP application might not be so robust as that of intrinsic PKGII expressed in the BF neurons (Werner et al., 2004). Nevertheless, in the control condition without PKG modulators, there was no apparent difference in the pH dependence of the scaled conductance between PKG-loaded HEK cells and cholinergic BF neurons (Fig. 8, compare continuous curves in *A*,*B*), and PKG inhibition shifted the pH dependence of the scaled conductance in the basic direction almost equally in PKG-loaded HEK cells and cholinergic BF neurons (Fig. 8, compare interrupted curves in *A*,*B*). These observations would indicate that there is no marked difference in the basal activity of PKG between PKG-loaded HEK cells and cholinergic BF neurons. If this is the case, there should be no marked difference in [cGMP] between them. Although [cGMP] in HEK cells is reported to be low (Bischof et al., 1997; Parkinson et al., 1999), [cGMP] may be dominated by [GTP] in the patch pipette as long as HEK cells maintain the activity of sGC (Bischof et al., 1997; Parkinson et al., 1999). Then, a similar basal PKG activity may be achieved by a similar basal sGC activity in HEK cells and cholinergic BF neu-

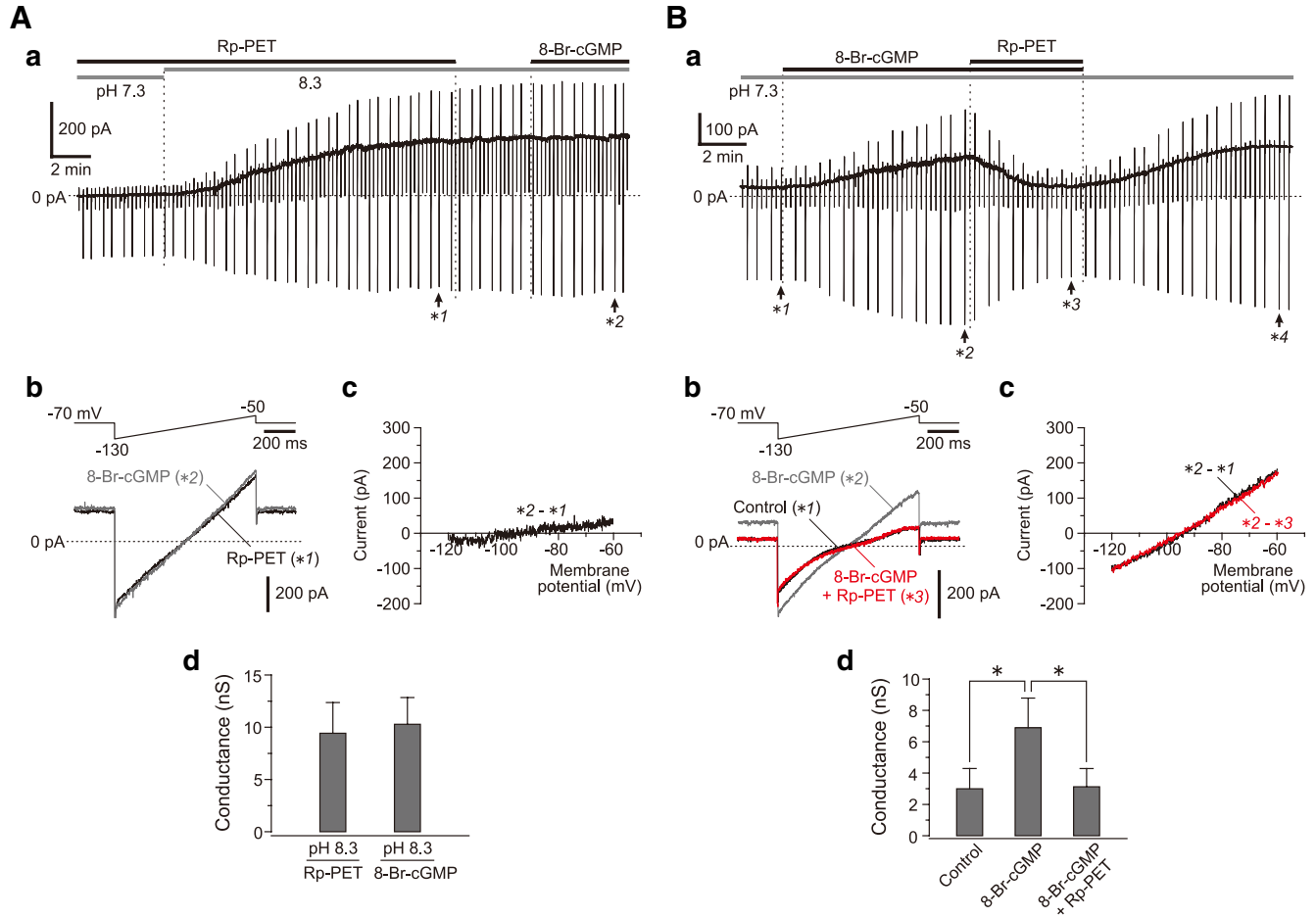

Figure 7. Rp-PET displays a lack of inhibition in the *I*-K_{leak} at pH 8.3. ***Aa***, A sample continuous recording of currents obtained in a cholinergic BF neuron following pH increase from 7.3 to 8.3 in the presence of Rp-PET and subsequently at pH 8.3 in the presence of 8-Br-cGMP after a brief washout of Rp-PET. Two black horizontal bars labeled with 20 μM Rp-PET and 200 μM 8-Br-cGMP represent the duration and timing of application of respective agents. ***Ab***, Top, Voltage command pulse. Bottom, Superimposed current traces obtained at the time points indicated with **1* and **2* in ***Aa***. ***Ac***, *I–V* relationship of 8-Br-cGMP-induced current obtained at pH 8.3 following application of 8-Br-cGMP after washout of Rp-PET (**2* − **1*). ***Ad***, The mean conductances ($n = 6$) at pH 8.3 in the presence of Rp-PET (9.4 ± 2.9 nS) and at pH 8.3 following the subsequent application of 8-Br-cGMP (10.3 ± 2.6 nS). ***Ba***, A sample continuous recording of currents at pH 7.3 obtained in a cholinergic BF neuron before and during application of 8-Br-cGMP, and during and after coapplication of 8-Br-cGMP and Rp-PET. Black horizontal bars represent the duration and timing of 200 μM 8-Br-cGMP and those of 20 μM Rp-PET application, respectively. ***Bb***, Top, Voltage command pulse. Bottom, Superimposed current traces obtained at the time points indicated with **1*, **2*, and **3* in ***Ba***. ***Bc***, *I–V* relationships of 8-Br-cGMP-induced current (**2* − **1*) and Rp-PET-sensitive current (**2* − **3*). ***Bd***, The mean conductances ($n = 6$) obtained before and during application of 8-Br-cGMP and during coapplication of 8-Br-cGMP and Rp-PET at pH 7.3. *$p < 0.001$ (§, *post hoc*).

rons, through the production of cGMP from GTP supplied equally from the patch pipette. It is natural that the difference in the PKG activity between HEK cells and cholinergic BF neurons becomes more apparent as the PKG activity is enhanced more by 8-Br-cGMP, presumably due to the difference in the robustness or efficiency between extrinsic and intrinsic PKG.

PKG bidirectionally shifts pH sensitivity profile of TASK1 currents

Neither KT5823 (Rp-PET) nor 8-Br-cGMP affected the minimum and maximum conductances in the TASK1 and K_{leak} channels respectively seen at pH 6.3 and 8.3 (Figs. 2–4, 6, and 7). Therefore, basic and acidic shifts in the pH sensitivity profiles of TASK1 currents caused by KT5823 and 8-Br-cGMP, respectively, may be brought about by a decrease and an increase in K_d, respectively (Fig. 8). Indeed, such changes in K_d value were revealed in the simulations of the scaled conductances measured from the TASK1 currents in HEK cells and the *I*-K_{leak} in cholinergic BF neurons by the Hill equation with a Hill coefficient of 2 for homodimeric TASK1 channels (Morton et al., 2003). PKG inhibition caused basic shifts in the pH sensitivity profiles of the TASK1 and K_{leak} conductances similarly by decreasing the K_d values, while the enhancement of PKG activity caused acidic shifts in the pH sensitivity profiles of the TASK1 and K_{leak} conductances similarly by increasing the K_d values (Fig. 8). Similar bidirectional modulations of pH sensitivity have been demonstrated by mutating K210 and H72 of TASK1 channels, which are located at extracellular sites on the pore (Morton et al., 2003). A mutation of K210 to asparagine increased the K_d value, while a mutation of H72 to asparagine decreased the K_d value, in comparison with WT TASK1 channels (Morton et al., 2003).

Mechanisms underlying pH-dependent inhibition of TASK channels

The *Drosophila* KCNK0, a member of the two-pore-domain K^+ channel (K_{2P}) family, displays the C-type gate closing that entails protein rearrangement of the outer mouth of the channel pore (Zilberberg et al., 2001), which was originally reported in voltage-gated K^+ channels such that they can be modulated by phosphorylation of their carboxy-terminal (Hoshi et al., 1991; Liu et al.,

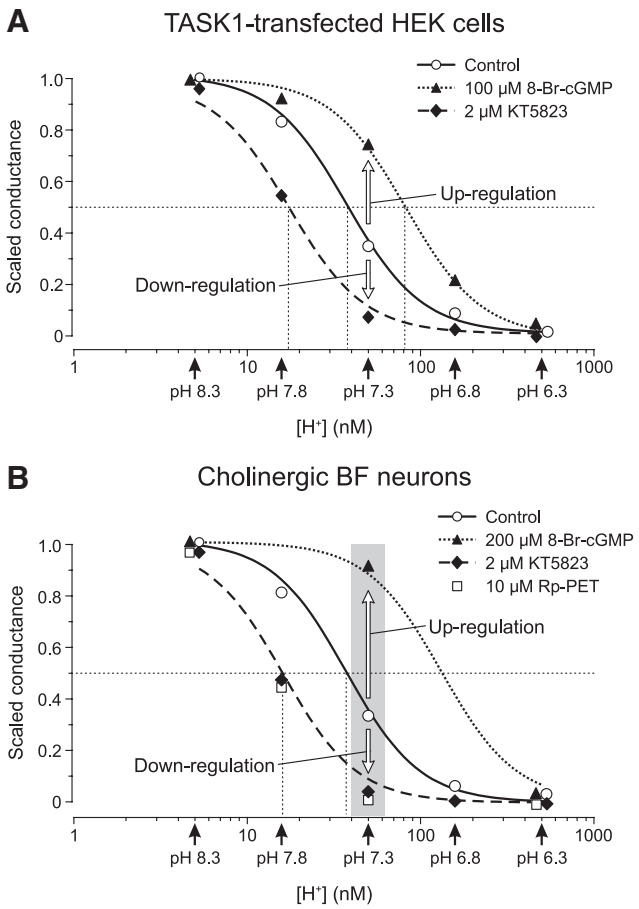

Figure 8. Modulation of pH-dependent inhibition of TASK1 currents and $I\text{-}K_{leak}$ in an identical manner dependent on PKG activity. ***A***, Filled diamonds, open circles, and filled triangles represent the mean scaled conductances of TASK1 currents at pH 6.3, 6.8, 7.3, 7.8, and 8.3 in the presence of KT5823, in the control condition and in the presence of 8-Br-cGMP, respectively. The interrupted, continuous, and dotted curves represent the simulated pH profiles of scaled conductances by using the Hill equation with a coefficient of 2, yielding the respective K_d values; 17 nM in the presence of KT5823, 37 nM in control condition and 82 nM in the presence of 8-Br-cGMP. ***B***, Filled diamonds, open squares, open circles, and filled triangles represent the scaled conductances of $I\text{-}K_{leak}$ in cholinergic BF neurons at pH 6.3, 6.8, 7.3, 7.8, and 8.3 in the presence of KT5823, in the presence of Rp-PET, in control condition and during application of 8-Br-cGMP, respectively. The interrupted, continuous, and dotted curves represent the simulated pH profiles of scaled conductances by using the Hill equation with a coefficient of 2, yielding the respective K_d values; 15 nM in the presence of KT5823, 35 nM in control condition, and approximately 113 nM in the presence of 8-Br-cGMP.

1996). Recently, it has also been reported that protonation of extracellular histidine residue of $K_{2P}2.1$ (TREK1) induces the closure of outer pore gate, i.e., the C-type gate closing (Cohen et al., 2008).

In TASK1 channels, the conductance was decreased by protonation of the pH sensors such as the extracellular histidine residue, H98, situated in the outer mouth of the channel pore, while this conductance decrease was considered to be due to proton block (Lopes et al., 2001; Morton et al., 2003). However, extracellular pH decreases did not significantly change the single channel conductance and the mean open time in TASK1 channels while decreasing the open probability (Kim et al., 1999). This observation is incompatible with the idea of the proton block, but in favor of the C-type gate closing, presumably due to the protonation of extracellular pH sensors. In the present study, the PKG modulation of the current responses was largely abolished or decreased by mutations of the pH sensors, H98N and K210N, in a manner inversely proportional to the potency of protonation of mutated pH sensor, suggesting that the modulatory effects of PKG are mediated by the activity of the pH sensors. Together, it is likely that PKG-mediated phosphorylation of an intracellular site on TASK1 channels alters the local environment of the pH sensor, such as H98, situated on the first pore domain of TASK1 channels to change its K_d value for protonation, thereby modulating the C-type gating.

The current responses at pH 6.3 were not markedly affected by application of 8-Br-cGMP/KT5823 both in H98N and K210N channels (Fig. 4), similar to the results obtained in WT TASK1 channels (Figs. 2 and 3). This suggests that the probability of C-type gate closing by protonation of pH sensors in TASK1 channels reaches maximum around pH 6. PKG modulation would alter the K_d value for protonation of TASK1 without affecting the minimum and maximum probabilities of C-type gate closing around pHs 8 and 6, respectively. The conductance decrease in H98N seen at pHs lower than 6 may be mediated by the proton blockade, which is known to be progressed in various cation channels by lowing the extracellular pH usually <6 (Hille, 2001), although the anomalous proton block is also known to occur even at the physiological pH range due to the anomalously high affinity for H^+ as reported in L-type Ca^{2+} channels (Chen et al., 1996). However, a further study on the single channel kinetics may be necessary to ascertain that the C-type gate closing, rather than the anomalous proton block, is the primary determinant of TASK1 channel activity induced in response to PKG modulation.

Modulations of K_d by PKG are not due to pH-dependent distribution of PKG modulators

There may be a possibility that Rp-PET and 8-Br-cGMP were less effective at basic pH than at neutral or acidic pH, which may also be viewed as "bidirectional modulations of the K_d value." This is because at basic pH, those solutes in the extracellular solution would be more ionized to become less membrane permeable than at neutral or acidic pH. Such a phenomenon is known as the partitioning of solutes across the lipid bilayer, which is influenced by the pH (Scherrer and Howard, 1977). However, a nonionized PKG inhibitor, KT5823, dissolved in a polar aprotic solvent of DMSO caused an almost same shift in the pH sensitivity profile of $I\text{-}K_{leak}$ as caused by Rp-PET (Fig. 8*B*, compare filled diamonds and open squares). This indicates that the membrane permeability of Rp-PET was not markedly affected by the changes in pH only ranged between 6.3 and 8.3. Furthermore, the ineffectiveness of 8-Br-cGMP on the $I\text{-}K_{leak}$ at pH 8.3 is completely compatible with the ineffectiveness of KT5823 on the $I\text{-}K_{leak}$ at pH 8.3, provided that the $I\text{-}K_{leak}$ at pH 8.3 is not affected by the activity of PKG. Together, these observations suggest that the partition of these solutes were not markedly affected by the changes in pH only ranged between 6.3 and 8.3. Thus, modulations of apparent K_d by PKG are not due to pH-dependent distribution of PKG modulators.

Modulation of TASK1-mediated $I\text{-}K_{leak}$ in cholinergic BF neurons

The $I\text{-}K_{leak}$ enhanced by NO-cGMP-PKG activation in the type II BF neurons was very similar to TASK1 current in its pH sensitivity (Kang et al., 2007; Toyoda et al., 2008). In the present study, the single-cell RT-PCR revealed that the type II neurons invariably express both TASK1 and ChAT mRNAs (Fig. 5*A*,*B*), and the immunohistochemistry demonstrated that ChAT-positive neurons were immunoreactive for TASK1 channels but not for TASK3 channels in the BF (Fig. 5*D*,*E*). These results are consis-

tent with the report that in MS/DB nuclei many neurons expressed moderate to abundant amount of TASK1 mRNA whereas there were only few neurons that abundantly express TASK3 mRNA (Karschin et al., 2001). Furthermore, the dynamic modulations of TASK1-like pH sensitivity of the $I\text{-}K_{leak}$ by PKG activation and inhibition (Fig. 8*B*) were entirely reconstituted in HEK cells expressing TASK1 channels (Fig. 8*A*). Therefore, it is strongly suggested that bidirectional modulations of NO-cGMP-PKG pathway dynamically regulate TASK1-mediated $I\text{-}K_{leak}$ at physiological pH by altering the local environment of the extracellular pH sensors of TASK1 channels to bidirectionally change their K_d values for protonation in cholinergic BF neurons.

References

Bayliss DA, Sirois JE, Talley EM (2003) The TASK family: two-pore domain background K^+ channels. Mol Interv 3:205–219.

Bischof G, Serwold TF, Machen TE (1997) Does nitric oxide regulate capacitative Ca influx in HEK 293 cells? Cell Calcium 21:135–142.

Brice A, Berrard S, Raynaud B, Ansieau S, Coppola T, Weber MJ, Mallet J (1989) Complete sequence of a cDNA encoding an active rat choline acetyltransferase: a tool to investigate the plasticity of cholinergic phenotype expression. J Neurosci Res 23:266–273.

Butt E, Nolte C, Schulz S, Beltman J, Beavo JA, Jastorff B, Walter U (1992) Analysis of the functional role of cGMP-dependent protein kinase in intact human platelets using a specific activator 8-para-chlorophenylthio-cGMP. Biochem Pharmacol 43:2591–2600.

Butt E, Pöhler D, Genieser HG, Huggins JP, Bucher B (1995) Inhibition of cyclic GMP-dependent protein kinase-mediated effects by (Rp)-8-bromo-PET-cyclic GMPS. Br J Pharmacol 116:3110–3116.

Chen XH, Bezprozvanny I, Tsien RW (1996) Molecular basis of proton block of L-type Ca^{2+} channels. J Gen Physiol 108:363–374.

Cohen A, Ben-Abu Y, Hen S, Zilberberg N (2008) A novel mechanism for human $K_{2P}2.1$ channel gating. Facilitation of C-type gating by protonation of extracellular histidine residues. J Biol Chem 283:19448–19455.

Furuta T, Koyano K, Tomioka R, Yanagawa Y, Kaneko T (2004) GABAergic basal forebrain neurons that express receptor for neurokinin B and send axons to the cerebral cortex. J Comp Neurol 473:43–58.

Goldstein SA, Bockenhauer D, O'Kelly I, Zilberberg N (2001) Potassium leak channels and the KCNK family of two-P-domain subunits. Nat Rev Neurosci 2:175–184.

Griffith WH, Matthews RT (1986) Electrophysiology of AChE-positive neurons in basal forebrain slices. Neurosci Lett 71:169–174.

Hidaka H, Kobayashi R (1992) Pharmacology of protein kinase inhibitors. Annu Rev Pharmacol Toxicol 32:377–397.

Hille B (2001) Ion channels of excitable membranes, Ed 3. Sunderland, MA: Sinauer.

Hopwood SE, Trapp S (2005) TASK-like K^+ channels mediate effects of 5-HT and extracellular pH in rat dorsal vagal neurones in vitro. J Physiol 568:145–154.

Hoshi T, Zagotta WN, Aldrich RW (1991) Two types of inactivation in Shaker K^+ channels: effects of alterations in the carboxy-terminal region. Neuron 7:547–556.

Kang D, Han J, Talley EM, Bayliss DA, Kim D (2004) Functional expression of TASK-1/TASK-3 heteromers in cerebellar granule cells. J Physiol 554: 64–77.

Kang Y, Dempo Y, Ohashi A, Saito M, Toyoda H, Sato H, Koshino H, Maeda Y, Hirai T (2007) Nitric oxide activates leak K^+ currents in the presumed cholinergic neuron of basal forebrain. J Neurophysiol 98:3397–3410.

Karschin C, Wischmeyer E, Preisig-Müller R, Rajan S, Derst C, Grzeschik KH, Daut J, Karschin A (2001) Expression pattern in brain of TASK-1, TASK-3, and a tandem pore domain K^+ channel subunit, TASK-5, associated with the central auditory nervous system. Mol Cell Neurosci 18:632–648.

Kim Y, Bang H, Kim D (1999) TBAK-1 and TASK-1, two-pore K^+ channel subunits: kinetic properties and expression in rat heart. Am J Physiol 277:H1669–H1678.

Kwan HY, Huang Y, Yao X (2004) Regulation of canonical transient receptor potential isoform 3 (TRPC3) channel by protein kinase G. Proc Natl Acad Sci U S A 101:2625–2630.

Lesage F (2003) Pharmacology of neuronal background potassium channels. Neuropharmacol 44:1–7.

Liu Y, Jurman ME, Yellen G (1996) Dynamic rearrangement of the outer mouth of a K^+ channel during gating. Neuron 16:859–867.

Lopes CM, Zilberberg N, Goldstein SA (2001) Block of Kcnk3 by protons. Evidence that 2-P-domain potassium channel subunits function as homodimers. J Biol Chem 276:24449–24452.

Markram H, Segal M (1990) Electrophysiological characteristics of cholinergic and non-cholinergic neurons in the rat medial septum-diagonal band complex. Brain Res 513:171–174.

Meuth SG, Budde T, Kanyshkova T, Broicher T, Munsch T, Pape HC (2003) Contribution of TWIK-related acid-sensitive K^+ channel 1 (TASK1) and TASK3 channels to the control of activity modes in thalamocortical neurons. J Neurosci 23:6460–6469.

Millar JA, Barratt L, Southan AP, Page KM, Fyffe RE, Robertson B, Mathie A (2000) A functional role for the two-pore domain potassium channel TASK-1 in cerebellar granule neurons. Proc Natl Acad Sci U S A 97: 3614–3618.

Morton MJ, O'Connell AD, Sivaprasadarao A, Hunter M (2003) Determinants of pH sensing in the two-pore domain K^+ channels TASK-1 and -2. Pflugers Arch 445:577–583.

Parkinson SJ, Jovanovic A, Jovanovic S, Wagner F, Terzic A, Waldman SA (1999) Regulation of nitric oxide-responsive recombinant soluble guanylyl cyclase by calcium. Biochemistry 38:6441–6448.

Patel AJ, Honoré E (2001) Properties and modulation of mammalian 2P domain K^+ channels. Trends Neurosci 24:339–346.

Saito M, Murai Y, Sato H, Bae YC, Akaike T, Takada M, Kang Y (2006) Two opposing roles of 4-AP-sensitive K^+ current in initiation and invasion of spikes in rat mesencephalic trigeminal neurons. J Neurophysiol 96:1887–1901.

Scherrer RA, Howard SM (1977) Use of distribution coefficients in quantitative structure-activity relationships. J Med Chem 20:53–58.

Sim JA, Allen TG (1998) Morphological and membrane properties of rat magnocellular basal forebrain neurons maintained in culture. J Neurophysiol 80:1653–1669.

Sirois JE, Lei Q, Talley EM, Lynch C 3rd, Bayliss DA (2000) The TASK-1 two-pore domain K^+ channel is a molecular substrate for neuronal effects of inhalation anesthetics. J Neurosci 20:6347–6354.

Talley EM, Lei Q, Sirois JE, Bayliss DA (2000) TASK-1, a two-pore domain K^+ channel, is modulated by multiple neurotransmitters in motoneurons. Neuron 25:399–410.

Talley EM, Solorzano G, Lei Q, Kim D, Bayliss DA (2001) CNS distribution of members of the two-pore-domain (KCNK) potassium channel family. J Neurosci 21:7491–7505.

Toyoda H, Saito M, Sato H, Dempo Y, Ohashi A, Hirai T, Maeda Y, Kaneko T, Kang Y (2008) cGMP activates a pH-sensitive leak K^+ current in the presumed cholinergic neuron of basal forebrain. J Neurophysiol 99:2126–2133.

Werner C, Raivich G, Cowen M, Strekalova T, Sillaber I, Buters JT, Spanagel R, Hofmann F (2004) Importance of NO/cGMP signalling via cGMP-dependent protein kinase II for controlling emotionality and neurobehavioural effects of alcohol. Eur J Neurosci 20:3498–3506.

White RE, Kryman JP, El-Mowafy AM, Han G, Carrier GO (2000) cAMP-dependent vasodilators cross-activate the cGMP-dependent protein kinase to stimulate BK_{Ca} channel activity in coronary artery smooth muscle cells. Circ Res 86:897–905.

Zilberberg N, Ilan N, Goldstein SA (2001) KCNK0: opening and closing the 2-P-domain potassium leak channel entails "C-type" gating of the outer pore. Neuron 32:635–648.